Research Square

Preprints are preliminary reports that have not undergone peer review.
They should not be considered conclusive, used to inform clinical practice,
or referenced by the media as validated information.

Depot- and Sex Specific Effects of the PTN/RPTPβ/ζ Axis on White Adipose Tissue Browning and Inflammatory Remodelling in Diet-Induced Obesity

Marta Inmaculada Sanz-Cuadrado
Universidad San Pablo-CEU, CEU Universities, Urbanización Montepríncipe
Julio Sevillano
Universidad San Pablo-CEU, CEU Universities, Urbanización Montepríncipe
María Gracia Sánchez-Alonso
Universidad San Pablo-CEU, CEU Universities, Urbanización Montepríncipe
Teresa Fontán-Baselga
Universidad San Pablo- CEU, CEU Universities, Urbanización Montepríncipe
Héctor Cañeque-Rufo
Universidad San Pablo-CEU, CEU Universities, Urbanización Montepríncipe
María Limones
Universidad San Pablo-CEU, CEU Universities, Urbanización Montepríncipe
José María Zapico
Universidad San Pablo-CEU, CEU Universities, Urbanización Montepríncipe
Beatriz de Pascual-Teresa
Universidad San Pablo-CEU, CEU Universities, Urbanización Montepríncipe
Gonzalo Herradón
Universidad San Pablo- CEU, CEU Universities, Urbanización Montepríncipe
María del Pilar Ramos-Álvarez
pramos@ceu.es

Universidad San Pablo-CEU, CEU Universities, Urbanización Montepríncipe

Research Article

Keywords: Pleiotrophin (PTN), Adipose tissue, Inflammation, High-fat diet-induced obesity, Browning, RPTPβ/ζ

Posted Date: September 28th, 2026

DOI: https://doi.org/10.21203/rs.3.rs-10979990/v1

License: This work is licensed under a Creative Commons Attribution 4.0 International License.
Read Full License

Additional Declarations: No competing interests reported.

Abstract

Metabolic syndrome is characterised by chronic low-grade inflammation and adipose tissue dysfunction. Pleiotrophin, a cytokine involved in tissue remodelling and energy metabolism, has emerged as a potential regulator of adipose tissue plasticity and systemic metabolic homeostasis. We investigated the role of pleiotrophin signalling in diet-induced obesity and adipose tissue inflammation, by genetic pleiotrophin deletion and pharmacological inhibition of RPTPβ/ζ phosphatase activity by MY10, a selective inhibitor that mimics pleiotrophin signalling. Male and female wild-type and pleiotrophin-deficient mice were fed a standard or a high-fat diet (60% kcal from fat) for three months. A parallel cohort of wild-type mice fed the standard or the high-fat diet received either vehicle or MY10. Adipose tissue morphology, fibrosis, inflammatory and thermogenic markers were analysed by histology, immunohistochemistry, qPCR and Western blotting. Pleiotrophin deletion attenuated high fat diet-induced weight gain, adipocyte hypertrophy and fibrosis, while promoting browning of white adipose tissue and enhancing thermogenic gene expression. Pleiotrophin-deficient mice showed reduced macrophage accumulation and elevated anti-inflammatory cytokine expression, particularly in subcutaneous adipose tissue. In contrast, MY10 treatment exacerbated adiposity and inflammation and suppressed browning-associated markers in a sex- and depot-dependent manner. Overall, these findings support a role for pleiotrophin in modulating adipose tissue inflammation and thermogenic programming during obesity: pleiotrophin deletion is associated with a protective phenotype, whereas pharmacological inhibition of RPTPβ/ζ phosphatase activity by MY10 aggravates obesity-associated adipose tissue dysfunction. Collectively, these observations identify the pleiotrophin–RPTPβ/ζ axis as a context-dependent regulator of adipose tissue remodelling and support its further investigation in obesity-associated metabolic dysfunction.

Key points

- *Ptn* deletion limits HFD-induced adipose expansion, fibrosis and inflammation
- *Ptn* deficiency enhances browning-associated markers in white adipose tissue
- MY10 promotes an adipose phenotype opposite to that observed after *Ptn* deletion
- Pleiotrophin-RPTPβ/ζ adipose remodelling varies by sex and adipose tissue depot

Introduction

Obesity has become a global epidemic with a significant socio-economic impact on healthcare systems [1, 2]. Its progression involves structural and functional alterations in adipose tissue, driven by excess nutrient and energy intake. This leads to the development of chronic, low-grade inflammation, known as metainflammation, which markedly disrupts metabolic homeostasis [3, 4]. These changes include adipocyte hypertrophy and hyperplasia, leading to an expansion of adipose tissue mass, as well as activation of resident immune cells [5–8], which release inflammatory mediators that sustain and self-amplify the metainflammatory state [4, 5, 8, 9]. This obesity-associated metainflammation has been

strongly linked to serious comorbidities, including type 2 diabetes mellitus, cardiovascular disease, and metabolic dysfunction-associated steatohepatitis (MASH) [8, 10].

White adipose tissue exists primarily in two anatomically and functionally distinct depots: subcutaneous (sWAT) and visceral adipose tissue (vWAT), which play divergent roles in the pathophysiology of obesity. sWAT, situated beneath the dermis, is predominantly composed of small, insulin-sensitive adipocytes with a high capacity for lipid uptake and triacylglycerol synthesis, and therefore serves a metabolically protective role [11]. In contrast, vWAT, located intra-abdominally around vital organs, consists of larger, hypertrophic adipocytes with reduced insulin sensitivity, impaired adipogenic potential and a pro-inflammatory profile characterised by increased macrophages infiltration and elevated secretion of cytokines such as TNF-α and IL-6 [12]. As the storage capacity of sWAT becomes limited during progressive adiposity, lipid accumulation shifts towards vWAT, which is strongly associated with insulin resistance, systemic inflammation, and increased risk of cardiometabolic disorders [13, 14]. WAT distribution is also sex-dependent. Typically, females accumulate subcutaneous fat more readily than males, who tend to show greater visceral deposition, the latter being more strongly associated with adverse metabolic outcomes [15].

Pleiotrophin (PTN) is a highly conserved cytokine of the heparin-binding growth factor family. Its expression is prominent during embryonic development and the early stages of life, but is tightly restricted in adulthood, except in contexts involving tissue repair, cell proliferation and angiogenesis [16–18]. Beyond these classical roles, PTN has emerged as an important regulator of metabolic homeostasis, contributing to the maintenance of insulin sensitivity and to the control of adipose tissue lipid turnover and brown adipose tissue thermogenesis [19, 20]. We have also demonstrated that PTN is essential for preserving pancreatic structural integrity, a key determinant of normal glucose tolerance [21]. Altogether, these observations suggest that PTN may be a relevant regulator of obesity-associated alterations in glucose homeostasis and lipid metabolism. However, whether PTN deficiency differentially affects individual adipose depots under severe diet-induced obesity, and whether these effects differ by sex, remains unclear.

Consistent with its role in metabolic regulation, a previous study conducted in female mice, showed that genetic deletion of *Ptn* protects against glucose intolerance and hepatic steatosis in a mouse model of overweight induced by a moderate high-fat diet (45% kcal from fat) [22]. Furthermore, we have very recently demonstrated that *Ptn* deletion protects against 60% HFD-induced hepatic steatosis, with a sexually dimorphic response characterized by greater protection in females than in males [23]. Building on these findings, the present study aims to investigate the role of PTN in adipose tissue expandability under a more severe obesogenic condition (a high-fat diet with 60% of energy derived from fat) and the contribution of sexual dimorphism to these effects. We hypothesise that *Ptn* deletion confers protection against HFD-induced adipose tissue inflammation, macrophage infiltration and metabolic dysfunction, potentially through enhanced tissue plasticity and adaptive thermogenic responses.

To further dissect the role of pleiotrophin signalling in obesity-related metabolic dysfunction, we also incorporated a pharmacological approach using MY10, a small synthetic molecule that selectively binds to the intracellular PD1 domain of the PTN receptor RPTPβ/ζ, inhibiting its phosphatase activity [24]. Because PTN itself inactivates RPTPβ/ζ, pharmacological inhibition of this phosphatase reproduces rather than opposes PTN signalling. Therefore, MY10 serves as a pharmacological tool to explore PTN-driven mechanisms mediated through the RPTPβ/ζ pathway [24], and its effects are expected to diverge from those of *Ptn* deletion. Accordingly, we investigated whether *Ptn* deletion differentially modulates adipose tissue expansion, inflammatory remodelling, fibrosis and browning across visceral and subcutaneous depots in male and female mice exposed to a 60% HFD and used MY10 in parallel to explore the involvement of RPTPβ/ζ signalling in these responses.

Materials and methods

Animal model

All animal procedures were conducted in accordance with the European Union Directive 2010/63/EU on the protection of laboratory animals and were approved by the Animal Research Committee of Universidad San Pablo-CEU and the Comunidad de Madrid (PROEX 140.3/22). *Ptn*-deficient mice ($Ptn^{-/-}$) were generated as previously described [25]. Female and male wild-type ($Ptn^{+/+}$) and $Ptn^{-/-}$ mice of the C57BL/6J strain were housed at 22 ± 1°C under a 12-hour light/dark cycle, with free access to food and water.

In the first experimental cohort, three-month-old female and male $Ptn^{+/+}$ and $Ptn^{-/-}$ mice were randomly assigned to a standard diet (STD; 18% kcal from fat, 58% from carbohydrate, and 24% from protein; Teklad 2918C, ENVIGO-INOTIV, Indianapolis, IN, USA) or a high-fat diet (HFD; D12492, 60% kcal from fat, 20% from carbohydrate, and 20% from protein; Ssniff Spezialdiäten GmbH, Soest, Germany) for three months (n = 7 mice per group).

Body surface temperature was measured weekly at noon in the dorsal region using the Body Temperature Scanner (SF-HANDHELD-80TA05 Safire 80×60 Therm; accuracy ± 0.5°C; Safire CCTV, Madrid, Spain). Three repeated measurements were taken per animal per session, and the average value was used for subsequent analyses.

In a second cohort, three-month-old female and male $Ptn^{+/+}$ mice were fed either the STD or the HFD for three months and treated every other day by intragastric gavage with either vehicle (Veh; 10% dehydrated ethanol, 20% polysorbate 80, 70% PEG-300) or MY10 (60 mg/kg), a selective inhibitor of the intracellular PD1 domain of RPTPβ/ζ that mimics the biological actions of PTN. The dose and administration schedule were based on previous *in vivo* studies with this compound [26].

After three months of dietary intervention, mice were fasted for 6 h and subsequently euthanised by decapitation. Adipose tissue depots were excised, weighed and either snap-frozen in liquid nitrogen and

stored at − 80°C or fixed in 4% paraformaldehyde. For the histological analysis, two white adipose tissue depots were selected: perigonadal adipose tissue, as a representative of visceral adipose tissue (vWAT), and posterior subcutaneous adipose tissue as representative of subcutaneous adipose tissue (sWAT).

Histological analysis

Perigonadal and subcutaneous adipose tissue were fixed in 4% paraformaldehyde, dehydrated and paraffin embedded. For histological analysis, 3-µm thick tissue sections were deparaffinised, rehydrated and stained with haematoxylin and eosin. Representative areas were acquired at 10× magnification by optical microscopy (Leica Biosystems, Barcelona, Spain).

Adipocyte morphology was quantified in a blinded manner using five non-consecutive sections per animal (n = 5 animals per group). Adipocyte number was expressed as number per mm^2, and the area was calculated in μm^2. Automated adipocyte segmentation and size quantification were performed with Adiposoft, using broad diameter limits to avoid size-based exclusion of adipocytes, followed by manual correction to ensure segmentation accuracy. Image analysis was performed using ImageJ 1.45 software (National Institutes of Health, Bethesda, MD, USA) in combination with the Adiposoft plugin (http://fiji.sc/Adiposoft). Frequency distribution histograms of adipocyte size were generated using SPSS Statistics software.

Fibrosis analysis

Adipose tissue fibrosis was assessed by picrosirius red staining and optical microscopy. Fibrosis quantification was performed in a blinded manner, on five sections per animal (n = 5 animals per group) captured at 10× magnification. Fibrosis was expressed as the percentage of picrosirius red–positive area relative to the total analysed area, using ImageJ 1.45 software.

Quantitative real-time PCR analysis

Total RNA was isolated from adipose tissue using the Total RNA Isolation Kit (Nzytech, Lisbon, Portugal), and first-strand cDNA was synthesised with the NZY First-Strand cDNA Synthesis Kit (Nzytech). Quantitative real-time PCR (qRT-PCR) was performed using the SYBR Green method (Quantimix Easy kit, Biotools, Madrid, Spain) on a CFX96 Real-Time PCR System (Bio-Rad, Hercules, CA, USA). Each sample was analysed in duplicate. mRNA levels were normalised to the geometric mean of the reference genes *Actb* and *Prdx1* and calculated by the $2^{-\Delta\Delta Ct}$ method [27]. For each gene, values across all experimental groups and fat depots were expressed relative to the mRNA detected in vWAT from male $Ptn^{+/+}$ mice fed the STD. The primer sequences are listed in Table 1. For clarity, genes are referred to throughout by their commonly used names; the corresponding official symbols are *Adgre1* (*F4/80*), *Itgax* (*Cd11c*) and *Ccl2* (*Mcp1*).

Table 1
Primer sets used for qPCR analysis

Gene	Primer forward	Primer reverse
Actb	5'-TGTTACCAACTGGGACGACA-3'	5'-GGGGTGTTGAAGGTCTCAAA-3'
Prdx1	5'-CCACACAGCTCTACAAGGACC-3'	5'-CGTTGTCCCGCTACTACGTTTC-3'
Arg1	5'-CTCCAAGCCAAAGTCCTTAGAG-3'	5'-AGGAGCTGTCATTAGGCACAT-3'
Cd11c	5'-TGAGAATCAGCTGAAGGAGAAGA-3'	5'-GGGGTACAAGAAGAAGGCACCTC-3'
Cidea	5'-GCCTGCAGGAACTTATCAGC-3'	5'-AGAACTCCTCTGTGTCCACCA-3'
Col6a1	5'-CATTGGCTAACATGACGCAG3'	5'-GAGTTAGCGATGTCCCTCAG-3'
F480	5'-CAGATACAGCAATGCCAAGCA-3'	5'-GATTGTGAAGGTAGCATTCACAAGTG-3'
Hoxc8	5’-AAGGACAAGGCCACTTAAAT-3’	5’-TCTGATACCGGCTGTAAGTTT-3’
Il6	5'-TAGTCCTTCCTACCCAATTTCC-3'	5'-TTGGTCCTTAGCCACTCCTTC-3'
Il10	5'-CGGGAAGACAATAACTGCACCC-3'	5'-CGGTTAGCAGTATGTTGTCCAGC-3'
Mcp1	5'-GGCTCAGCCAGATGCAGTTAA-3'	5'-CCTACTATTGGGATCATCTTGCT-3'
Pparγ2	5’-GATGCACTGCCTATGAGCACTT-3’	5’-AGAGGTCCACAGAGCTGATTCC-3’
Ptn	5’- TTGGGGAGAATGTGACCTCAATAC-3’	5’- GGCTTGGAGATGGTGACAGTTTTC-3’
Ptprz1	5’- GCCTGGATTGGGCTAATGGA-3’	5’- TGAAACTCCTCCGCTGACAC-3’
Ucp1	5'-GGATTGGCCTCTACGACTCA-3'	5'-TAAGCCGGCTGAGATCTTGT-3'

Immunohistochemical analysis

Paraffin-embedded adipose tissue sections were deparaffinised, rehydrated and subjected to antigen retrieval by boiling in 10 mM sodium citrate buffer (pH 6.0) containing 0.05% Tween-20 for 20 minutes. Endogenous peroxidase activity was quenched with 3% hydrogen peroxide for 30 minutes. Sections were blocked for 30 minutes with blocking serum (VECTASTAIN ABC-HRP kit, Vector Laboratories, PK-4001, Newark, CA, USA) and incubated overnight with the primary antibodies against F4/80 and UCP-1 (all references and dilutions in Table 2). Subsequently, sections were incubated with the appropriate secondary antibody (VECTASTAIN ABC-HRP kit), and immunoreactivity was visualised with 3,3'-diaminobenzidine as the chromogen (Sigma-Aldrich, St. Louis, MO, USA). Sections incubated without primary antibody served as negative controls. Staining was assessed qualitatively on five sections per animal (n = 5 animals per group).

Electrophoresis and Western Blot

Perigonadal and subcutaneous adipose tissue samples were homogenised in a pH 7.4 buffer containing 30 mM HEPES, 5 mM EDTA, 1% Triton X-100, 0.5% sodium deoxycholate, 8 mM Na_3VO_4, 1 mM NaF (Sigma-Aldrich, St. Louis, MO, USA), and 2 mM of the protease inhibitor mixture Pefabloc (Roche Diagnostics, Barcelona, Spain). Total protein concentration was determined by the Pierce BCA Protein assay kit (Thermo-Scientific, Waltham, MA, USA).

Equal amounts of total protein (30 µg) were separated by SDS-PAGE and transferred onto PVDF membranes (Amersham-GE Healthcare, Amersham, UK). Membranes were blocked for 30 minutes at room temperature with 10% non-fat dry milk, then washed three times with TBST (10 mM Tris-HCl, 0.15 M NaCl, and 0.5% Tween, pH = 8) and incubated overnight at 4ºC with primary antibodies against UCP1 and vinculin (details are listed in Table 2). Membranes were then washed and incubated for 30 minutes at room temperature with the appropriate horseradish peroxidase-conjugated secondary antibodies (anti-mouse or anti-rabbit, 1:10,000; Sigma-Aldrich). Proteins were visualised by chemiluminescence (Amersham ECL Western Blotting Detection system, Cytiva, Marlborough, MA, USA) on the ChemiDoc Imaging System (Bio-Rad Laboratories, Hercules, CA, USA), and band intensities were quantified by densitometry with ImageJ.

Table 2
Antibodies used for immunohistochemistry and western blotting analysis

Antibody	Dilution	Reference
anti-F4/80 [SP115] (IHC)	1:100	Abcam ab111101, Cambridge, UK
anti-UCP1 [EPR20381] (IHC)	1:2000	Abcam ab209483, Cambridge, UK
anti-UCP1 (WB)	1:1000	GeneTex GTX112784, Irvine, CA, USA
anti-Vinculin (WB)	0.1 µg/µl	Sigma-Aldrich V9264, St. Louis, MO, USA
Anti-rabbit IgG-Peroxidase (WB)	1:10000	Sigma-Aldrich A0545, St. Louis, MO, USA
Anti-mouse IgG-Peroxidase (WB)	1:10000	Sigma-Aldrich A9044, St. Louis, MO, USA

Statistical analysis

Data are presented as mean ± standard error of the mean (SEM). Normality and homogeneity of variance were verified by Shapiro–Wilk and Levene tests, respectively. Longitudinal body weight data were analysed by repeated-measures analysis of variance (ANOVA), with time as the within-subject factor and the corresponding experimental variables as between-subject factors. Depending on the experimental design, endpoint variables were analysed by three-way or four-way ANOVA as appropriate, to evaluate the main effects and interactions among sex, diet, genotype, treatment or adipose tissue depot. To facilitate the interpretation of diet-, genotype- or treatment-dependent effects, additional two-way ANOVAs were performed separately for each sex and adipose tissue depot. Post hoc multiple comparisons were performed with Bonferroni correction; effect sizes are reported as partial η^2.

Significance was set at $p < 0.05$. Outliers were identified and excluded using Grubbs' test in GraphPad Prism.

All analyses were carried out using GraphPad Prism version 8.0 (GraphPad Software, San Diego, CA, USA) or IBM SPSS Statistics (IBM, Armonk, NY, USA), depending on the complexity of the analysis.

Results

Ptn deletion attenuates HFD-induced body weight gain and adipose tissue expansion in both sexes

Body weight throughout the experimental period was lower in both male and female *Ptn*$^{-/-}$ mice than in their *Ptn*$^{+/+}$ counterparts under standard diet (STD) conditions. As expected, HFD feeding markedly increased body weight in all groups and, after three months of dietary intervention, body weight remained significantly higher in HFD-*Ptn*$^{+/+}$ than in HFD-*Ptn*$^{-/-}$ mice, of both sexes (Fig. 1a, b). Food intake did not differ significantly between genotypes on either diet (Fig. 1g), indicating that the lower weight gain of *Ptn*$^{-/-}$ mice was not attributable to reduced energy intake.

Statistical analysis identified genotype and diet as the main determinants of body weight, with highly significant effects and large effect sizes ($p < 0.001$, $\eta^2 > 0.65$ for both). A significant genotype × diet interaction was also observed with a substantial effect size, indicating that the impact of HFD on body weight depends strongly on genotype. In contrast, sex did not significantly influence body weight gain. All details of the statistical analysis are shown in **Supplementary Table 1**.

In parallel, *Ptn* and *Ptprz1* (RPTPβ/ζ) expression was assessed to determine whether dietary conditions modulate the PTN/RPTPβ/ζ signalling axis. Neither *Ptn* nor *Ptprz1* mRNA was significantly altered by HFD feeding; as expected, *Ptn* was undetectable in *Ptn*$^{-/-}$ animals (**Supplementary Fig. 1**).

We next analysed white adipose tissue mass and distribution after three months with the diet, in visceral (vWAT: perigonadal, retroperitoneal and mesenteric) and subcutaneous (sWAT) depots. Although HFD increased the mass of all WAT depots, adiposity was significantly lower in *Ptn*$^{-/-}$ than in *Ptn*$^{+/+}$ animals (Fig. 1c-f), and perigonadal fat remained the predominant visceral depot across all groups. Three-way ANOVA revealed a predominant role of genotype and diet over sex in determining adipose tissue expansion (**Supplementary Table 1**).

Among all depots, sWAT showed the greatest expansion in response to HFD in *Ptn*$^{+/+}$ mice (8.12-fold in males and 15.31-fold in females), exceeding that of every visceral depot, in which perigonadal (2.75-fold in males; 5.73-fold in females) and retroperitoneal (3.17-fold in males and 6.48-fold in females) increased more than mesenteric fat (2.62-fold in males and 3.59-fold in females). These results are consistent with sWAT, acting as the primary site of lipid storage under HFD conditions, particularly in females, in line with its lipid-buffering role.

Ptn deletion markedly attenuated HFD-induced adipose tissue expansion in all depots, being significantly lower than in $Ptn^{+/+}$ counterparts; subcutaneous fat expanded only 3.53-fold in males and 2.26-fold in females, and in visceral depots the retroperitoneal expanded 1.92-fold in males, 2.99-fold in females; the perigonadal, 2.11-fold in males, 2.86-fold in females; the mesenteric, 2.06-fold in males, 2.12-fold in females. These results underscore a role of PTN in promoting adipose tissue growth under obesogenic conditions, with its absence conferring partial protection against excessive fat accumulation.

Ptn deletion restrains adipocyte hypertrophy and attenuates adipose tissue fibrosis

Morphological analysis of perigonadal (as a visceral depot) and subcutaneous adipose tissues was performed to evaluate the effects of *Ptn* deletion and HFD feeding on adipocyte size and tissue fibrosis.

Quantitative analysis of haematoxylin-eosin-stained sections confirmed that adipocytes in sWAT were smaller than those in vWAT (Fig. 2, **Supplementary Table 2**). Pleiotrophin deletion was associated with a higher proportion of small adipocytes and, although HFD feeding induced adipocyte hypertrophy in both depots across genotypes, this effect was smaller in $Ptn^{-/-}$ than in $Ptn^{+/+}$ mice, and adipocytes from $Ptn^{-/-}$ mice remained consistently smaller than those of wild-type animals. No statistically significant sex-related differences were observed.

Adipose tissue fibrosis, characterised by increased collagen deposition, was evaluated by picrosirius red staining (**Fig. 3**). HFD feeding significantly increased picrosirius red-positive collagen area in adipose tissue from $Ptn^{+/+}$ mice, indicating enhanced fibrosis. In contrast, although HFD feeding induced adipocyte hypertrophy in $Ptn^{-/-}$ mice, it did not result in a significant increase in collagen deposition or fibrotic area. These findings suggest that *Ptn* deletion attenuates HFD-induced adipose tissue fibrosis.

Fibrosis was significantly influenced by sex, with higher collagen deposition in males than in females, although the corresponding effect size indicates only a moderate contribution. Adipose depot, genotype and diet exerted a stronger effect on fibrosis than sex alone ($p < 0.001$ for all variables), with the adipose depot accounting for the greatest magnitude of effect ($\eta^2 > 0.19$). All statistical details are shown in **Supplementary Table 3**.

To further assess extracellular matrix, *Col6a1* mRNA was quantified. As expected, HFD feeding increased *Col6a1* expression in $Ptn^{+/+}$ mice. In contrast, $Ptn^{-/-}$ mice exhibited lower *Col6a1* mRNA after three months of HFD feeding, in both subcutaneous and visceral depots, than $Ptn^{+/+}$ mice (**Fig. 3c**). Statistical analysis revealed significant effects of sex, diet and genotype on *Col6a1* mRNA levels ($p < 0.001$ for all comparisons), with genotype and diet accounting for the greatest magnitudes of effect ($\eta^2 > 0.23$ and $\eta^2 > 0.19$, respectively).

Ptn deficiency is associated with reduced macrophage markers and a less inflammatory adipose tissue profile

To evaluate how *Ptn* deletion influences the effect of HFD feeding on the inflammatory state of white adipose tissue, we measured mRNA of markers associated with M1-like and M2-like macrophages, together with pro- and anti-inflammatory cytokines in both sWAT and vWAT depots. Distinct inflammatory profiles emerged according to diet, genotype, sex and fat depot.

As shown in Fig. 4a–d, the expression of the pro-inflammatory cytokines (*Mcp1* and *Il6*) and the macrophage-markers (*F4/80* and *Cd11c*) was significantly affected by both genotype and diet (see **Supplementary Table 4**). HFD feeding markedly increased these mRNA in the white adipose tissue of $Ptn^{+/+}$ mice, whereas the response was notably attenuated in $Ptn^{-/-}$ animals, suggesting that *Ptn* deficiency protects against HFD-induced adipose tissue inflammation. The significant effect of genotype on these markers reinforces this interpretation, while the significant interaction terms further indicate sex- and depot-dependent differences in this response (**Supplementary Table 4**).

Moreover, representative F4/80 immunostaining showed a pattern qualitatively consistent with the mRNA data. HFD feeding markedly increased F4/80-positive staining in $Ptn^{+/+}$ mice, indicative of enhanced macrophage infiltration and more pronounced in vWAT than in sWAT, whereas $Ptn^{-/-}$ mice showed weaker F4/80 staining under HFD conditions. (Fig. 4g).

Anti-inflammatory markers also exhibited genotype-, depot- and sex-dependent differences (Fig. 4e, f). *Arg1* and *Il10* were significantly influenced by adipose tissue depot, with higher expression in sWAT, particularly in $Ptn^{-/-}$ mice, even under HFD conditions. The significant main effect of genotype on both markers also suggests a shift towards an anti-inflammatory phenotype in the absence of PTN, especially in sWAT, further supporting depot-specific immune modulation. In *Arg1*, genotype exerted the strongest main effect ($\eta^2 > 0.48$), whereas sex also explained a considerable proportion of the variance ($\eta^2 > 0.20$). Moreover, a significant and large genotype and sex interaction was observed ($\eta^2 > 0.49$). *Il10* mRNA did not show a significant sex-dependent effect, consistent with sexual dimorphism in adipose tissue immune responses.

Ptn deletion is associated with a thermogenic, and browning-like phenotype in white adipose tissue

Analysis of thermogenic markers in white adipose tissue revealed a marked upregulation of *Ucp1* and *Cidea* mRNA levels in $Ptn^{-/-}$ mice compared to $Ptn^{+/+}$ controls (Fig. 5a, b).

Sex significantly affected *Ucp1* expression, but its contribution was smaller than that of depot and genotype, the latter being the major source of variation ($\eta^2 > 0.20$, $\eta^2 > 0.28$, $\eta^2 > 0.48$, for sex, depot and genotype, respectively (see in **Supplementary Table 5** for complete statistical details). Significant effects of genotype and depot on *Cidea* mRNA were observed, although their effect sizes were more modest than those observed for *Ucp1* ($\eta^2 > 0.11$, $\eta^2 > 0.12$, for depot and genotype, respectively). These results suggest that, while sex and depot contribute to variability in thermogenic gene expression, genotype represents the primary determinant.

Analysis of *Pparg2* mRNA revealed significant effects of diet, genotype, and adipose tissue depot (Fig. 5c). In contrast, *Hoxc8* expression was significantly affected only by genotype, with $Ptn^{-/-}$ mice exhibiting lower mRNA levels than $Ptn^{+/+}$ controls, regardless of diet or adipose tissue depot (Fig. 5d).

These findings were supported at the protein level by increased UCP1 detected by Western Blotting (Fig. 5e) and immunostaining (Fig. 5g), indicating an induction of a browning phenotype in the absence of PTN. Consistently, $Ptn^{-/-}$ mice showed higher body surface temperature than $Ptn^{+/+}$ controls with a significant effect of genotype (**Supplementary Table 6**). The heatmap in Fig. 5f further showed consistently higher body temperatures in $Ptn^{-/-}$ mice in agreement with elevated UCP1 expression and consistent with an enhanced browning-like phenotype.

MY10 treatment increases body weight and adipose tissue expansion, particularly under high-fat diet conditions

To explore the involvement of RPTPβ/ζ signalling further, $Ptn^{+/+}$ male and female mice were treated with MY10 and fed either a STD or a HFD for three months, after which body and adipose tissue weights were assessed (Fig. 6).

First, *Ptn* and *Ptprz1* mRNA levels were analysed to determine whether MY10 treatment altered the expression of components of the PTN/RPTPβ/ζ signalling axis. Neither *Ptn* nor *Ptprz1* mRNA was significantly affected by MY10 treatment (**Supplementary Fig. 1**).

In contrast to *Ptn* deletion, pharmacological inhibition of RPTPβ/ζ with MY10 significantly increased body weight in mice fed the STD, an effect exacerbated by combined HFD and MY10 (Fig. 6a, b). Treatment and sex had significant effects ($\eta^2 > 0.34$, $\eta^2 > 0.36$, for treatment and sex, respectively), although the primary determinant was the diet ($\eta^2 > 0.88$; all statistical details in **Supplementary Table 7**). Food intake was comparable between vehicle- and MY10-treated groups (Fig. 6g).

Consistent with these findings, HFD feeding and MY10 treatment increased adipose tissue mass, with the greatest effects observed in mice co-treated with MY10 and HFD (Fig. 6c-f). Three-way ANOVA demonstrated significant effects of sex, treatment and diet on fat mass (see **Supplementary Table 7**). MY10 treatment also altered adipose tissue distribution across visceral and subcutaneous depots, an effect consistently amplified by HFD. In vWAT, MY10 significantly increased perigonadal, retroperitoneal, and mesenteric depots in both sexes (Fig. 6c, d), with perigonadal fat showing the largest response (2.66-fold in males and 2.30-fold in females under STD, rising to 5.20-fold and 4.78-fold, respectively, under HFD). Retroperitoneal and mesenteric depots showed a similar trend, that was less pronounced in males than in females. MY10 treatment likewise significantly increased sWAT mass in both sexes (1.80-fold in males and 2.0 in females under STD; 5.34-fold and 4.4-fold, respectively under HFD) (Fig. 6e, f **and Supplementary Table 7**). Collectively, MY10 promotes adipose tissue expansion in both visceral and subcutaneous depots, with effects accentuated under obesogenic conditions and modest, depot-specific differences between sexes.

MY10 treatment is associated with adipocyte hypertrophy and fibrotic remodelling in white adipose tissue

MY10 treatment increased adipocyte size in both vWAT and sWAT (Fig. 7). This effect was already evident under STD conditions and was further enhanced by HFD, indicating that MY10 promotes adipocyte hypertrophy, particularly in the context of dietary obesity. Median adipocyte areas and statistical analyses are provided in **Supplementary Tables 8 and 9**.

In parallel, picrosirius red staining revealed increased collagen deposition in adipose tissue from MY10-treated mice, indicating enhanced fibrosis. This fibrotic response was more pronounced under HFD conditions, consistent with a greater combined effect of MY10 treatment and dietary challenge (Fig. 8). *Col6a1* expression showed a more depot- and sex-specific pattern, with significant increases mainly observed in females, particularly in vWAT and in sWAT from MY10-HFD female mice (Fig. 8c).

MY10 exacerbates adipose tissue inflammation and reduces thermogenic markers

To evaluate the impact of MY10 treatment on adipose tissue inflammation, we quantified the mRNA of key inflammatory markers in vWAT and sWAT from $Ptn^{+/+}$ mice fed either STD or HFD and treated with vehicle or MY10.

MY10 treatment significantly increased the mRNA levels of the inflammatory markers *Mcp1* and *Il6* and of the macrophage-related markers *F4/80* and *Cd11c*, in both vWAT and sWAT, and these effects were further enhanced by HFD (Fig. 9a-d). Significant sex- and depot-dependent differences were observed for several of these markers. Regarding sex, male mice showed higher expression than females, particularly *Mcp1, Il6*, and *Cd11c*, ($p < 0.001$, for these markers; $\eta^2 > 0.44$; $\eta^2 > 0.17$; $\eta^2 > 0.23$, respectively). With respect to fat depots, all transcripts examined differed significantly between visceral and subcutaneous fat, with effect sizes indicating a strong depot-specific influence particularly of *Il6, F4/80*, and *Cd11c* ($\eta^2 > 0.39$; $\eta^2 > 0.26$; $\eta^2 > 0.40$, respectively; all analysis in **Supplementary Table 10**). These results indicate that MY10 exacerbates HFD-induced adipose tissue inflammation, with a stronger pro-inflammatory effect in the subcutaneous depot.

In addition, MY10 reduced the expression of anti-inflammatory markers *Arg1* and *Il10* (Fig. 9e, f) particularly in female mice. Furthermore, male mice fed the HFD and treated with MY10 exhibited lower *Il10* mRNA than their vehicle-treated HFD counterparts. These effects were supported by significant sex effects ($p < 0.001$, $\eta^2 > 0.29$ for both markers) as well as strong depot effects ($p < 0.001$, $\eta^2 > 0.38$). Together, these findings suggest a sex- and depot-specific pattern of inflammatory marker expression and immune regulation, likely reflecting differential responses of resident immune cell populations to MY10 treatment and dietary conditions.

Finally, the thermogenic markers *Ucp1* and *Cidea* were evaluated (Fig. 9g, h). Despite considerable inter-individual variability, particularly for *Ucp1*, MY10 treatment consistently downregulated mRNA of both markers in vWAT and sWAT of mice under both STD and HFD. These findings are opposite in direction to those obtained in PTN-deficient mice and, are therefore consistent with the proposed opposing effects of MY10 treatment and pleiotrophin deletion in the regulation of adipose tissue thermogenic programming.

Discussion

During obesity, excess energy storage promotes adipocyte enlargement, fat redistribution and adipose tissue remodelling [28]. Although sWAT initially acts as a major lipid-buffering depot, progressive adiposity may favour lipid accumulation in visceral depots, which are more strongly associated with insulin resistance and cardiovascular risk [12].

Previous studies from our group showed that *Ptn* deletion attenuates liver metabolic alterations induced by HFD feeding, although these findings were largely restricted to female mice exposed to a moderate-fat diet (45% kcal from fat) [22]. More recently, we demonstrated that *Ptn* deletion also protects against hepatic steatosis induced by a more severe dietary challenge (60% kcal from fat), revealing a sexually dimorphic response characterized by greater protection in females than in males [23]. Building upon these findings, the present study was designed to further investigate the sex-dependent effects of *Ptn* deletion under 60% HFD conditions, with particular emphasis on adipose tissue depot-specific responses. In parallel, the MY10 treatment allowed us to probe the involvement of RPTPβ/ζ phosphatase activity in these metabolic adaptations.

Consistent with the obesogenic effects of HFD, body weight and the weight of WAT, including sWAT and vWAT compartments, increased in both $Ptn^{+/+}$ and $Ptn^{-/-}$ mice, although the effect was less pronounced in *Ptn*-deficient animals. In $Ptn^{+/+}$ mice, sWAT showed the greatest expansion, exceeding that observed in all vWAT depots analysed. This finding reinforces the proposed role of sWAT as a major lipid-buffering depot, with its expansion potentially limiting ectopic lipid accumulation and metabolic dysfunction [12]. In contrast, *Ptn* deletion markedly reduced adipose tissue expansion, which is consistent with previous observations in *Ptn*-deficient mice [20], even under dietary fat overload with a 45% HFD [22].

Adipose depots differ functionally; sWAT adipocytes are generally smaller and have a greater capacity for fatty acid uptake and triglyceride synthesis, whereas vWAT shows higher infiltration of pro-inflammatory macrophages and greater production of cytokines such as MCP1 and IL-6 [14], contributing to inflammation, adipose dysfunction and systemic metabolic disturbance [5, 29]. In this line, we found that adipocytes in sWAT were smaller than those in vWAT across genotypes and sexes. HFD increased adipocyte size, fibrosis and collagen deposition in both depots of $Ptn^{+/+}$ mice, but these changes were attenuated in $Ptn^{-/-}$ animals, which retained smaller adipocytes, particularly in sWAT. Female $Ptn^{-/-}$ mice did not show a significant increase in sWAT mass after HFD exposure, suggesting a sex-specific limitation of subcutaneous fat expansion in the absence of PTN. Consistently, *Ptn* deletion

was associated with lower *Col6a1* mRNA and reduced fibrosis, processes typically linked to chronic adipose tissue inflammation in obesity [5, 29].

Given the established relationship between obesity and adipose tissue inflammation, we assessed macrophage infiltration and key pro- and anti-inflammatory markers. We found that the inflammatory response was strongly influenced by diet, sex and genotype, with clear differences between sWAT and vWAT.

HFD was associated with a more pronounced macrophage-related inflammatory profile in vWAT, characterised by increased *Cd11c* and *Mcp1* expression, together with adipocyte hypertrophy. These features are consistent with sustained immune activation and with the established link between visceral fat inflammation and systemic insulin resistance [28, 30]. In contrast, sWAT showed a milder response than vWAT, with lower macrophage-associated inflammation in males and relatively higher *Arg1* and *Il10* expression, consistent with an M2-like marker profile and with the metabolically protective role of this depot. Our data also reveal sexual dimorphism in adipose tissue inflammation. Male mice showed a more pronounced inflammatory phenotype in vWAT, with higher *F4/80, Cd11c*, *Mcp1* and *Il6* and lower *Arg1* and *Il10* expression, whereas female mice showed a more balanced or anti-inflammatory profile, particularly in sWAT. These observations are consistent with reports of partial female protection against HFD-induced metabolic dysfunction and with sex hormone-related differences in immune regulation and extracellular matrix remodelling [31], adipose tissue distribution [32–34], and fat depot expandability and browning capacity [32, 35].

Our findings also support a depot- and sex-dependent role for PTN in promoting adipose tissue inflammation. MY10 increased pro-inflammatory markers, particularly in sWAT under HFD conditions, especially in males. Conversely, *Ptn* deletion attenuated or even abolished the HFD-induced increase in *Mcp1, Il6, F4/80* and *Cd11c* in both WAT depots and increased the expression of *Il10* and *Arg1* in sWAT, suggesting an active engagement of anti-inflammatory pathways that may contribute to mitigating the inflammatory response. This depot-specific pattern was apparent under both STD and HFD in the sWAT of $Ptn^{-/-}$ mice, reinforcing the protective role of *Ptn* deletion against obesity-associated inflammation.

Analysis of thermogenic markers revealed a genotype-dependent increase in browning-associated markers in white adipose tissue. Whereas wild-type mice displayed minimal UCP1 immunoreactivity, consistent with a predominantly white adipocyte phenotype, $Ptn^{-/-}$ mice showed increased expression of *Cidea*, a lipid droplet-associated protein enriched in thermogenic adipocytes, and *Ucp1*, consistent with enhanced thermogenic programming and with our previous observations in $Ptn^{-/-}$ mice under other metabolic conditions [20, 22]. In parallel, *Ptn* deletion was associated with reduced *Pparg2* and *Hoxc8* expression. Although PPARg is essential for adipogenesis, reduced expression of the *Pparg2* isoform has been associated with adipose tissue remodelling and acquisition of beige adipocyte characteristics in specific physiological contexts [36]. Likewise, decreased expression of *Hoxc8*, a transcriptional repressor of thermogenic gene programmes, may facilitate UCP1 induction and the development of beige adipocyte features within WAT [37].

UCP1 induction was most pronounced in sWAT, together with morphological features of beige adipocytes such as smaller, multilocular lipid droplets, consistent with the recognised browning capacity of this depot [20, 22]. These effects appeared sex-dependent, as female *Ptn*$^{-/-}$ mice showed more pronounced *Ucp1* mRNA and protein, suggesting an enhanced thermogenic response. This agrees with reports indicating that females display a greater propensity for adipose tissue browning, potentially mediated by oestrogen-dependent signalling [38, 39]. Overall, although depot- and sex-related differences were observed, genotype accounted for a markedly larger effect size.

UCP1, a hallmark of brown and beige adipocytes, drives mitochondrial uncoupling, dissipating energy as heat and increasing energy expenditure [40, 41]. Accordingly, increased UCP1 expression in adipocytes and increased body surface temperature in *Ptn*$^{-/-}$ are consistent with a shift in energy balance towards greater energy dissipation. Although body surface temperature is only an indirect proxy of thermogenic activity, our previous study, in which energy expenditure was directly assessed by indirect calorimetry, demonstrated that six-month-old female *Ptn*$^{-/-}$ mice exhibited greater cold-induced thermogenesis than age-matched *Ptn*$^{+/+}$ controls [20]. These findings support the present results and suggest that thermogenic capacity is enhanced in PTN-deficient mice. This thermogenic phenotype may contribute to their reduced fat accumulation, lower body weight gain and attenuated metainflammation under HFD.

MY10 inhibits RPTPβ/ζ phosphatase activity by binding to its PD1 domain and, although MY10 and PTN interact with distinct sites on RPTPβ/ζ, MY10 mimics the inhibitory effect of PTN [24]. We therefore hypothesised that MY10 would produce effects opposite to those observed in *Ptn*-deficient mice. Consistent with this, MY10 significantly increased body weight in both sexes, an effect exacerbated under HFD and more pronounced in male mice. Furthermore, MY10 treatment also increased sWAT and vWAT mass, with the greatest accumulation observed in the MY10-treated mice on a HFD. These findings contrast with the reduced adiposity and limited fat mass expansion of *Ptn*-deficient mice, supporting the idea that MY10 mimics PTN actions through RPTPβ/ζ signalling and thereby promotes lipid storage in WAT in a sex-dependent manner.

In parallel, MY10 treatment increased adipocyte size and collagen deposition even under standard diet conditions. These effects were further exacerbated by HFD, indicating that RPTPβ/ζ inhibition promotes adipocyte hypertrophy and fibrotic remodelling in an obesogenic context.

Accordingly, MY10-treated *Ptn*$^{+/+}$ mice showed increased *Cd11c* and *Il6* expression, particularly in sWAT, consistent with a more pronounced pro-inflammatory macrophage-associated profile. MY10 also reduced the anti-inflammatory markers *Arg1* and *Il10*, particularly in females. As these genes are associated with alternatively activated M2-like macrophages and inflammation resolution, their suppression suggests that MY10 both promotes pro-inflammatory signalling and impairs compensatory anti-inflammatory pathways. Sex-related differences were also apparent in the inflammatory profile. Males showed higher pro-inflammatory marker expression after MY10 regardless of diet, whereas females showed a comparable increase mainly when MY10 was combined with HFD, suggesting that the response to RPTPβ/ζ inhibition becomes evident in females only under an additional metabolic stressor.

Together, these findings indicate that the influence of RPTPβ/ζ signalling on adipose tissue inflammation is context-dependent varying with adipose depot, sex, and dietary conditions.

As hypothesised, MY10 appears to mimic PTN-like signalling and was associated with reduced expression of thermogenic and browning-associated markers, as shown by lower *Ucp1* and *Cidea* expression in vWAT and sWAT under both standard and HFD conditions. This pattern is consistent with an impaired adaptive thermogenic programme and may contribute to the increased weight gain observed in these animals. These findings contrast with those observed in *Ptn*-deficient mice, which display enhanced expression of browning-associated and thermogenic markers together with a more pronounced thermogenic phenotype.

Taken together, the observed pattern is consistent with HFD-induced increases in *Mcp1* expression and pro-inflammatory macrophage-associated markers in vWAT, particularly in males, potentially contributing to local inflammation and fibrotic remodelling, whereas sWAT, particularly in females, retained a less pro-inflammatory, M2-like profile that may contribute to limit inflammation and preserve metabolic homeostasis. These results underscore the role of PTN in obesity-related adipose tissue dysfunction, as its deletion attenuates metainflammation in parallel with enhanced browning-associated and thermogenic markers. Conversely, inhibition of RPTPβ/ζ phosphatase activity by MY10 aggravated obesity-associated adipose tissue dysfunction by increasing body weight, adiposity, and inflammation while reducing thermogenic marker expression, with a generally less pronounced adverse phenotype in females.

In summary, our pharmacological findings support the involvement of RPTPβ/ζ phosphatase activity in the adipose phenotype associated with PTN signalling. Collectively, our results identify the PTN/RPTPβ/ζ axis as a context-dependent modulator of obesity-associated adipose remodelling and inflammation and underscore the importance of considering both adipose tissue depot and sex as key biological variables.

Declarations

Funding

This research was funded by grants from the Ministerio de Ciencia, Innovación y Universidades of Spain (PID2021-123865OB-I00/MICIU/ AEI/10.13039/501100011033/FEDER, UE and PDI2025-172972OB-I00) to MPR-A and GH and by Comunidad de Madrid (P2022/BMD-7227) to MPR-A. MS was supported by a predoctoral research contract funded by the Comunidad de Madrid under the 2022 call for grants for the recruitment of predoctoral researchers in training (Orden 3789/2022), and by the CEU-Santander Grant (Ayudas a la Contratación de Jóvenes Investigadores CEU-Santander, academic year 2022/2023) and was a recipient of CEU-Santander mobility grant.

Competing interests

The authors declare that the research was conducted in the absence of any commercial or financial relationships that could be construed as a potential conflict of interest.

Ethics approval

The animal study was approved by the Animal Research Committee of CEU San Pablo University and by Comunidad de Madrid (PROEX 140.3/22). The study was conducted in accordance with the local legislation and institutional requirements.

Data availability

The datasets generated and/or analysed during the current study are available from the corresponding author on reasonable request.

Clinical Trial number

not applicable.

Author Contributions

Marta Inmaculada Sanz-Cuadrado: Writing-original draft, Writing-review and editing, Visualization, Methodology, Investigation, Formal analysis, and Data curation.

Julio Sevillano: Writing-original draft, Writing-review and editing, Visualization, Validation, Supervision, Formal analysis, and Data curation.

María Gracia Sánchez-Alonso: Writing-review and editing, Methodology and Supervision.

Teresa Fontán-Baselga: Methodology, Investigation and Writing-review and editing.

Hector Cañeque-Rufo: Methodology, Investigation and Writing-review and editing.

María Limones: Methodology; Writing-review and editing.

José María Zapico: Methodology; Resources and Writing-review and editing.

Beatriz de Pascual-Teresa: Methodology; Resources and Writing-review and editing.

Gonzalo Herradón: Conceptualization, Project administration, Funding acquisition, and Writing-review and editing.

María del Pilar Ramos-Álvarez: Conceptualization, Supervision, Project administration, Funding acquisition, Writing-original draft, Writing-review and editing, Visualization.

References

1. NCD Risk Factor Collaboration (NCD-RisC) (2024) Worldwide trends in underweight and obesity from 1990 to 2022: a pooled analysis of 3663 population-representative studies with 222 million children, adolescents, and adults. Lancet 403:1027–1050. https://doi.org/10.1016/s0140-6736(23)02750-2
2. World Obesity Federation (2025) World Obesity Atlas 2025. London, UK
3. Hotamisligil GS (2017) Inflammation, metaflammation and immunometabolic disorders. Nature 542:177–185. https://doi.org/10.1038/nature21363
4. Russo S, Kwiatkowski M, Govorukhina N, Bischoff R, Melgert BN (2021) Meta-Inflammation and Metabolic Reprogramming of Macrophages in Diabetes and Obesity: The Importance of Metabolites. Front Immunol 12:746151. https://doi.org/10.3389/fimmu.2021.746151
5. Kawai T, Autieri MV, Scalia R (2021) Adipose tissue inflammation and metabolic dysfunction in obesity. Am J Physiol Cell Physiol 320:C375–c391. https://doi.org/10.1152/ajpcell.00379.2020
6. Li C, Xu MM, Wang K, Adler AJ, Vella AT, Zhou B (2018) Macrophage polarization and meta-inflammation. Transl Res 191:29–44. https://doi.org/10.1016/j.trsl.2017.10.004
7. Weisberg SP, McCann D, Desai M, Rosenbaum M, Leibel RL, Ferrante AW Jr. (2003) Obesity is associated with macrophage accumulation in adipose tissue. J Clin Invest 112:1796–1808. https://doi.org/10.1172/jci19246
8. Zatterale F, Longo M, Naderi J, Raciti GA, Desiderio A, Miele C et al (2019) Chronic Adipose Tissue Inflammation Linking Obesity to Insulin Resistance and Type 2 Diabetes. Front Physiol 10:1607. https://doi.org/10.3389/fphys.2019.01607
9. Gregor MFGS, Hotamisligil (2011) Inflammatory mechanisms in obesity. Annu Rev Immunol 29. https://doi.org/10.1146/annurev-immunol-031210-101322. :415 – 45
10. Charles-Messance H, Mitchelson KAJ, De Marco Castro E, Sheedy FJ, Roche HM (2020) Regulating metabolic inflammation by nutritional modulation. J Allergy Clin Immunol 146:706–720. https://doi.org/10.1016/j.jaci.2020.08.013
11. Zwick RK, Guerrero-Juarez CF, Horsley V, Plikus MV (2018) Anatomical, Physiological, and Functional Diversity of Adipose Tissue. Cell Metab 27:68–83. https://doi.org/10.1016/j.cmet.2017.12.002
12. Ibrahim MM (2010) Subcutaneous and visceral adipose tissue: structural and functional differences. Obes Rev 11:11–18. https://doi.org/10.1111/j.1467-789X.2009.00623.x
13. Xie W, Hong Z, Li B, Huang B, Dong S, Cai Y et al (2024) Influence of glucagon-like peptide-1 receptor agonists on fat accumulation in patients with diabetes mellitus and non-alcoholic fatty liver disease or obesity: A systematic review and meta-analysis of randomized control trials. J Diabetes Complications 38:108743. https://doi.org/10.1016/j.jdiacomp.2024.108743
14. Vishvanath LRK, Gupta (2019) Contribution of adipogenesis to healthy adipose tissue expansion in obesity. J Clin Invest 129:4022–4031. https://doi.org/10.1172/jci129191
15. Stranahan AM, Guo D-H, Yamamoto M, Hernandez CM, Khodadadi H, Baban B et al (2022) Sex Differences in Adipose Tissue Distribution Determine Susceptibility to Neuroinflammation in Mice

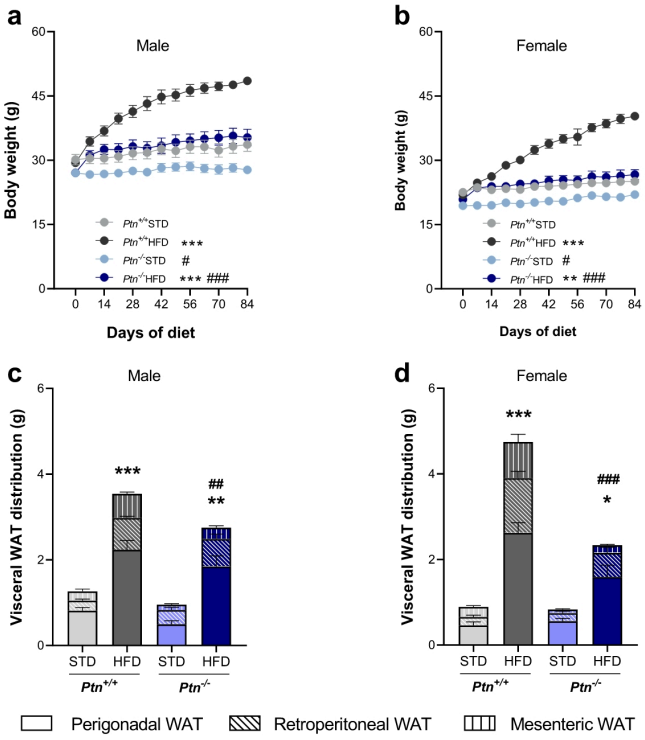
With Dietary Obesity. Diabetes 72:245–260. https://doi.org/10.2337/db22-0192

16. Deuel TF, Zhang N, Yeh HJ, Silos-Santiago I, Wang ZY (2002) Pleiotrophin: a cytokine with diverse functions and a novel signaling pathway. Arch Biochem Biophys 397:162–171. https://doi.org/10.1006/abbi.2001.2705
17. Wang X (2020) Pleiotrophin: Activity and mechanism. Adv Clin Chem 98:51–89. https://doi.org/10.1016/bs.acc.2020.02.003
18. Xu C, Zhu S, Wu M, Han W, Yu Y (2014) Functional receptors and intracellular signal pathways of midkine (MK) and pleiotrophin (PTN). Biol Pharm Bull 37:511–520. https://doi.org/10.1248/bpb.b13-00845
19. Ballesteros-Pla C, Sánchez-Alonso MG, Pizarro-Delgado J, Zuccaro A, Sevillano J, Ramos-Álvarez MP (2023) Pleiotrophin and metabolic disorders: insights into its role in metabolism. Front Endocrinol (Lausanne) 14:1225150. https://doi.org/10.3389/fendo.2023.1225150
20. Sevillano J, Sánchez-Alonso MG, Zapatería B, Calderón M, Alcalá M, Limones M et al (2019) Pleiotrophin deletion alters glucose homeostasis, energy metabolism and brown fat thermogenic function in mice. Diabetologia 62:123–135. https://doi.org/10.1007/s00125-018-4746-4
21. Ballesteros-Pla C, Sevillano J, Sánchez-Alonso MG, Limones M, Pita J, Zapatería B et al (2024) Constitutive Pleiotrophin Deletion Results in a Phenotype with an Altered Pancreatic Morphology and Function in Old Mice. Int J Mol Sci 25:10960. https://doi.org/10.3390/ijms252010960
22. Zuccaro A, Zapatería B, Sánchez-Alonso MG, Haro M, Limones M, Terrados G et al (2021) Pleiotrophin Deficiency Induces Browning of Periovarian Adipose Tissue and Protects against High-Fat Diet-Induced Hepatic Steatosis. Int J Mol Sci 22:9261. https://doi.org/10.3390/ijms22179261
23. Cañeque-Rufo H, Zuccaro A, Sanz-Cuadrado MI, Ruin F, Olivera-Rodríguez Á, Pizarro-Delgado J et al (2026) Deletion of Pleiotrophin protects against high-fat diet-induced liver metabolic disease, independently of the sexual dimorphism in dietary response. Mol Biomed 7:146. https://doi.org/10.1186/s43556-026-00547-9
24. Pastor M, Fernández-Calle R, Di Geronimo B, Vicente-Rodríguez M, Zapico JM, Gramage E et al (2018) Development of inhibitors of receptor protein tyrosine phosphatase β/ζ (PTPRZ1) as candidates for CNS disorders. Eur J Med Chem 144:318–329. https://doi.org/10.1016/j.ejmech.2017.11.080
25. Amet LE, Lauri SE, Hienola A, Croll SD, Lu Y, Levorse JM et al (2001) Enhanced hippocampal long-term potentiation in mice lacking heparin-binding growth-associated molecule. Mol Cell Neurosci 17:1014–1024. https://doi.org/10.1006/mcne.2001.0998
26. Fernández-Calle R, Galán-Llario M, Gramage E, Zapatería B, Vicente-Rodríguez M, Zapico JM et al (2020) Role of RPTPβ/ζ in neuroinflammation and microglia-neuron communication. Sci Rep 10:20259. https://doi.org/10.1038/s41598-020-76415-5
27. Livak KJTD, Schmittgen (2001) Analysis of Relative Gene Expression Data Using Real-Time Quantitative PCR and the 2 – ΔΔCT Method. Methods 25:402–408. https://doi.org/10.1006/meth.2001.1262

28. Longo M, Zatterale F, Naderi J, Parrillo L, Formisano P, Raciti GA et al (2019) Adipose Tissue Dysfunction as Determinant of Obesity-Associated Metabolic Complications. Int J Mol Sci 20:2358. https://doi.org/10.3390/ijms20092358
29. Ashik T, Lee V, Atanes P, Persaud SJ (2022) Alterations in mouse visceral adipose tissue mRNA expression of islet G-protein-coupled receptor ligands in obesity. Diabet Med 39:e14978. https://doi.org/10.1111/dme.14978
30. Olefsky JMCK, Glass (2010) Macrophages, inflammation, and insulin resistance. Annu Rev Physiol 72. https://doi.org/10.1146/annurev-physiol-021909-135846. :219 – 46
31. Grove KL, Fried SK, Greenberg AS, Xiao XQ, Clegg DJ (2010) A microarray analysis of sexual dimorphism of adipose tissues in high-fat-diet-induced obese mice. Int J Obes 34:989–1000. https://doi.org/10.1038/ijo.2010.12
32. Medrikova D, Jilkova ZM, Bardova K, Janovska P, Rossmeisl M, Kopecky J (2012) Sex differences during the course of diet-induced obesity in mice: adipose tissue expandability and glycemic control. Int J Obes 36:262–272. https://doi.org/10.1038/ijo.2011.87
33. Fried SK, Lee M-J, Karastergiou K (2015) Shaping fat distribution: New insights into the molecular determinants of depot- and sex-dependent adipose biology. Obesity 23:1345–1352. https://doi.org/10.1002/oby.21133
34. Palmer BFDJ, Clegg (2015) The sexual dimorphism of obesity. Mol Cell Endocrinol 402:113–119. https://doi.org/10.1016/j.mce.2014.11.029
35. Cohen P, Levy JD, Zhang Y, Frontini A, Kolodin DP, Svensson KJ et al (2014) Ablation of PRDM16 and beige adipose causes metabolic dysfunction and a subcutaneous to visceral fat switch. Cell 156:304–316. https://doi.org/10.1016/j.cell.2013.12.021
36. Li D, Zhang F, Zhang X, Xue C, Namwanje M, Fan L et al (2016) Distinct functions of PPARγ isoforms in regulating adipocyte plasticity. Biochem Biophys Res Commun 481:132–138. https://doi.org/10.1016/j.bbrc.2016.10.152
37. Pilkington A-C, Paz HA, Wankhade UD (2021) Beige Adipose Tissue Identification and Marker Specificity—Overview. Front Endocrinol (Lausanne) 12:599134. https://doi.org/10.3389/fendo.2021.599134
38. De Jesus ANBA, Henry (2023) The role of oestrogen in determining sexual dimorphism in energy balance. J Physiol 601:435–449. https://doi.org/10.1113/JP279501
39. Martínez de Morentin PB, González-García I, Martins L, Lage R, Fernández-Mallo D, Martínez-Sánchez N et al (2014) Estradiol Regulates Brown Adipose Tissue Thermogenesis via Hypothalamic AMPK. Cell Metabol 20:41–53. https://doi.org/10.1016/j.cmet.2014.03.031
40. Jagtap UA, Paul (2023) UCP1 activation: Hottest target in the thermogenesis pathway to treat obesity using molecules of synthetic and natural origin. Drug Discov Today 28:103717. https://doi.org/10.1016/j.drudis.2023.103717
41. Mills EL, Harmon C, Jedrychowski MP, Xiao H, Gruszczyk AV, Bradshaw GA et al (2022) Cysteine 253 of UCP1 regulates energy expenditure and sex-dependent adipose tissue inflammation. Cell Metab

34:140–157e8. https://doi.org/10.1016/j.cmet.2021.11.003

Figures



g

Experimental group	Sex	Food intake	
		Mean	SEM
Ptn $^{+/+}$ STD	Male	3,55	0,12
Ptn $^{+/+}$ HFD	Male	3,05	0,13
Ptn $^{-/-}$ STD	Male	3,28	0,20
Ptn $^{-/-}$ HFD	Male	3,21	0,44
Ptn $^{+/+}$ STD	Female	3,05	0,10
Ptn $^{+/+}$ HFD	Female	2,93	0,17
Ptn $^{-/-}$ STD	Female	3,25	0,65
Ptn $^{-/-}$ HFD	Female	3,21	0,19

Figure 1

Effects of *Ptn* deletion and HFD feeding on body weight and white adipose tissue distribution. Body weight of male (**a**) and female (**b**) $Ptn^{+/+}$ (grey symbols) and $Ptn^{-/-}$ (blue symbols) mice fed a standard diet (STD) or a high-fat diet (HFD) for three months. Distribution of visceral adipose tissue (perigonadal, retroperitoneal and mesenteric depots) in (**c**) male and (**d**) female mice. Subcutaneous adipose tissue mass in (**e**) male and (**f**) female mice. (**g**) Food intake during the 3-month dietary intervention. Data are shown as mean ± SEM (n = 7 mice per group). Statistical significance is indicated as follows: $*p < 0.05$; $**p < 0.01$; $*** p < 0.001$ for diet effects (HFD vs. STD within the same genotype), and $^{\#}p < 0.05$; $^{\#\#}p < 0.01$; $^{\#\#\#}p < 0.001$ for genotype effects ($Ptn^{+/+}$ vs. $Ptn^{-/-}$ within the same dietary condition).

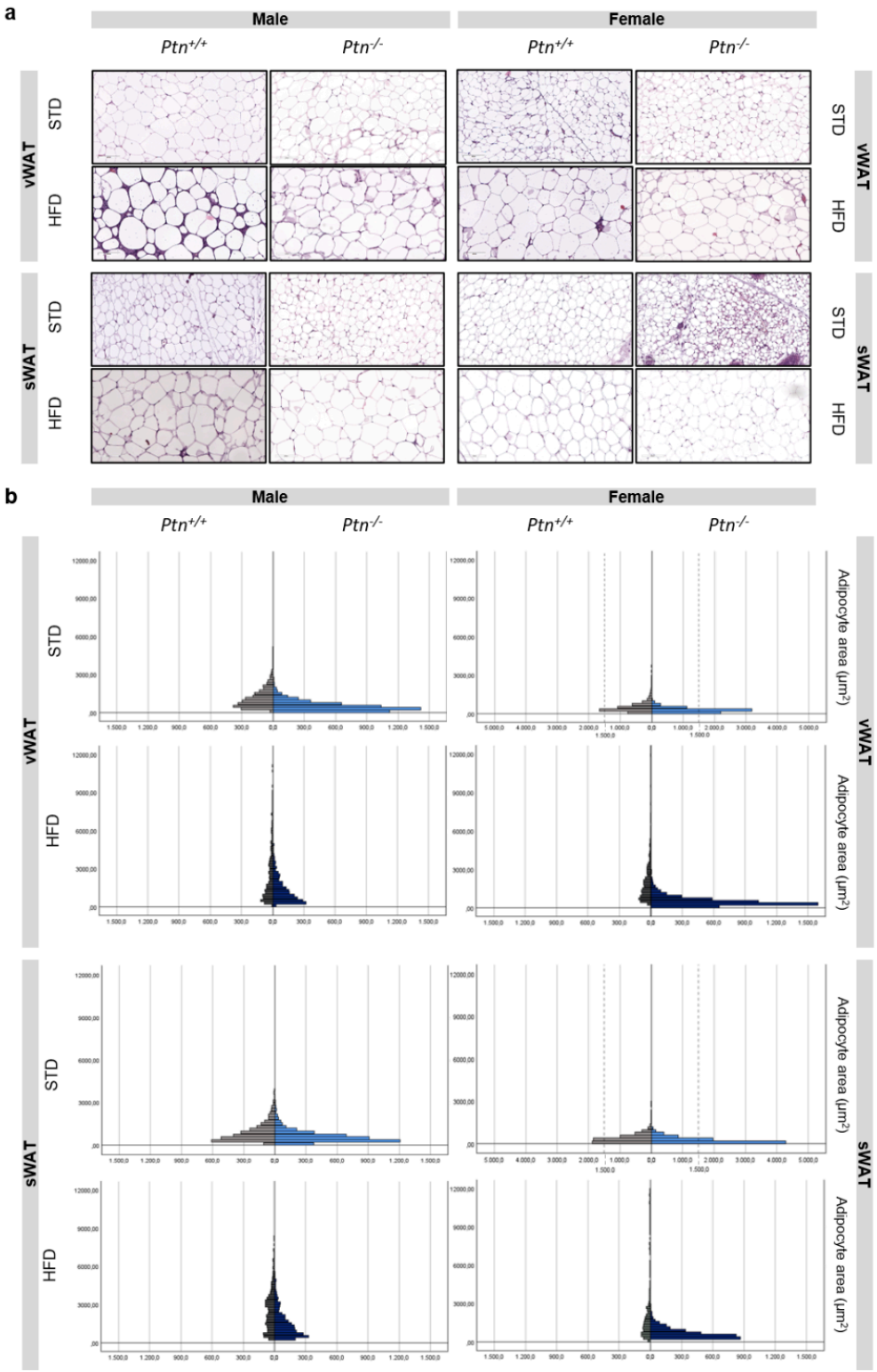


Figure 2

Effects of *Ptn* deletion and HFD feeding on morphology and number of adipocytes of visceral (perigonadal) and subcutaneous adipose tissue depots. (**a**) Representative sections of visceral perigonadal and subcutaneous adipose tissue stained with haematoxylin-eosin (10× magnification). (**b**) Distribution of the number and area (µm^2) of adipocytes of perigonadal and subcutaneous adipose

tissue of male *Ptn*$^{+/+}$ (grey) and *Ptn*$^{-/-}$ (blue) mice fed with STD and HFD for three months. (n = 5 mice/group).

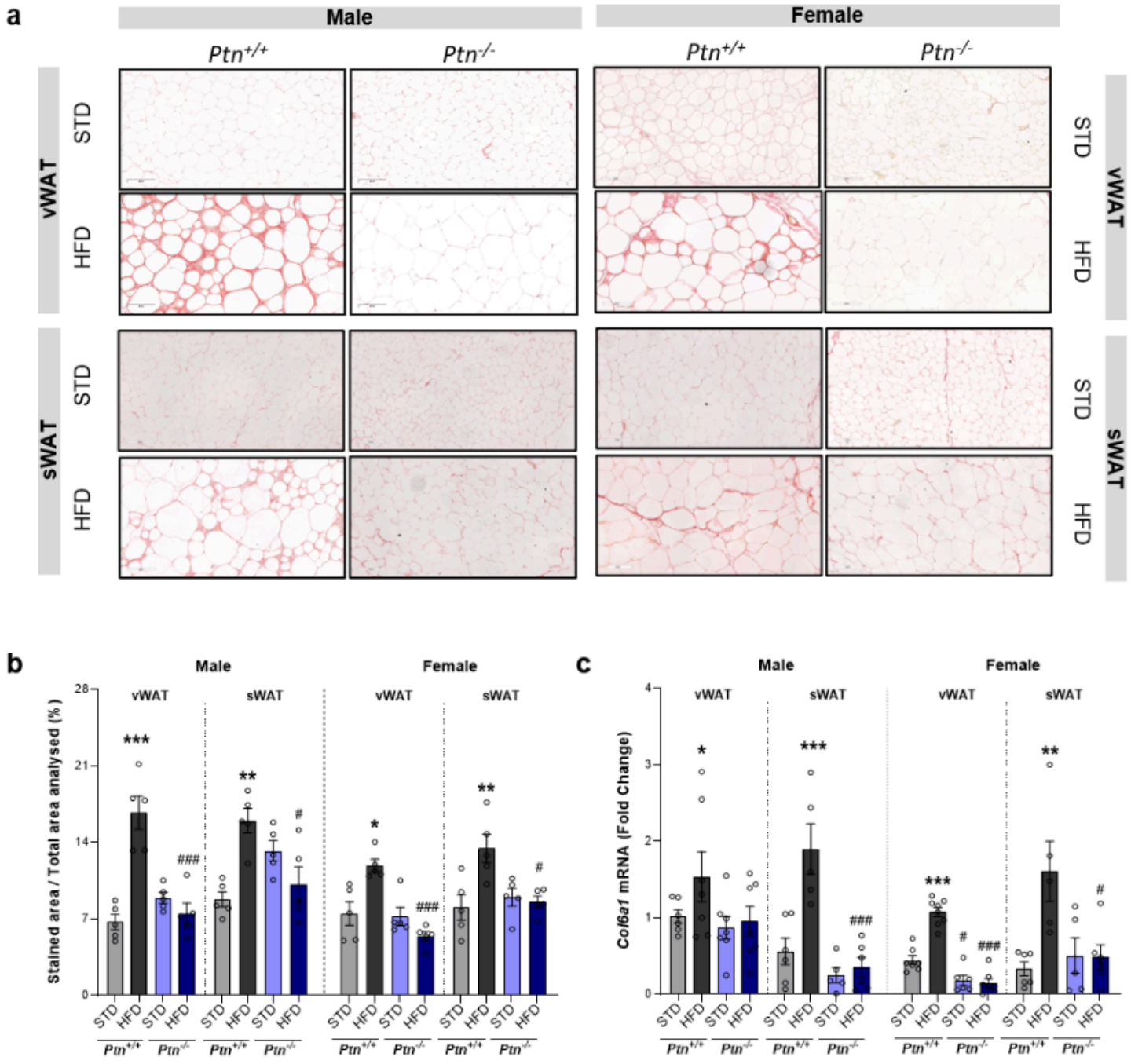


Figure 3

Effects of *Ptn* deletion and HFD feeding on fibrosis and extracellular matrix remodelling in white adipose tissue. (**a**) Histological section of visceral and subcutaneous adipose tissue with picrosirius red staining (10x magnification, scale bar 200µm). (**b**) Stained area relative to the total tissue area. (**c**) *Col6a1* mRNA measured by qPCR. Data are shown as mean ± SEM of n = 5 mice per group. *$p < 0.05$; **p

< 0.01; ***p < 0.001 for differences in the effect of HFD feeding within $Ptn^{+/+}$ or $Ptn^{-/-}$ mice. $^{\#}p$ < 0.05; $^{\#\#}p$ < 0.01; $^{\#\#\#}p$ < 0.001 for differences regarding genotype between $Ptn^{+/+}$ and $Ptn^{-/-}$.

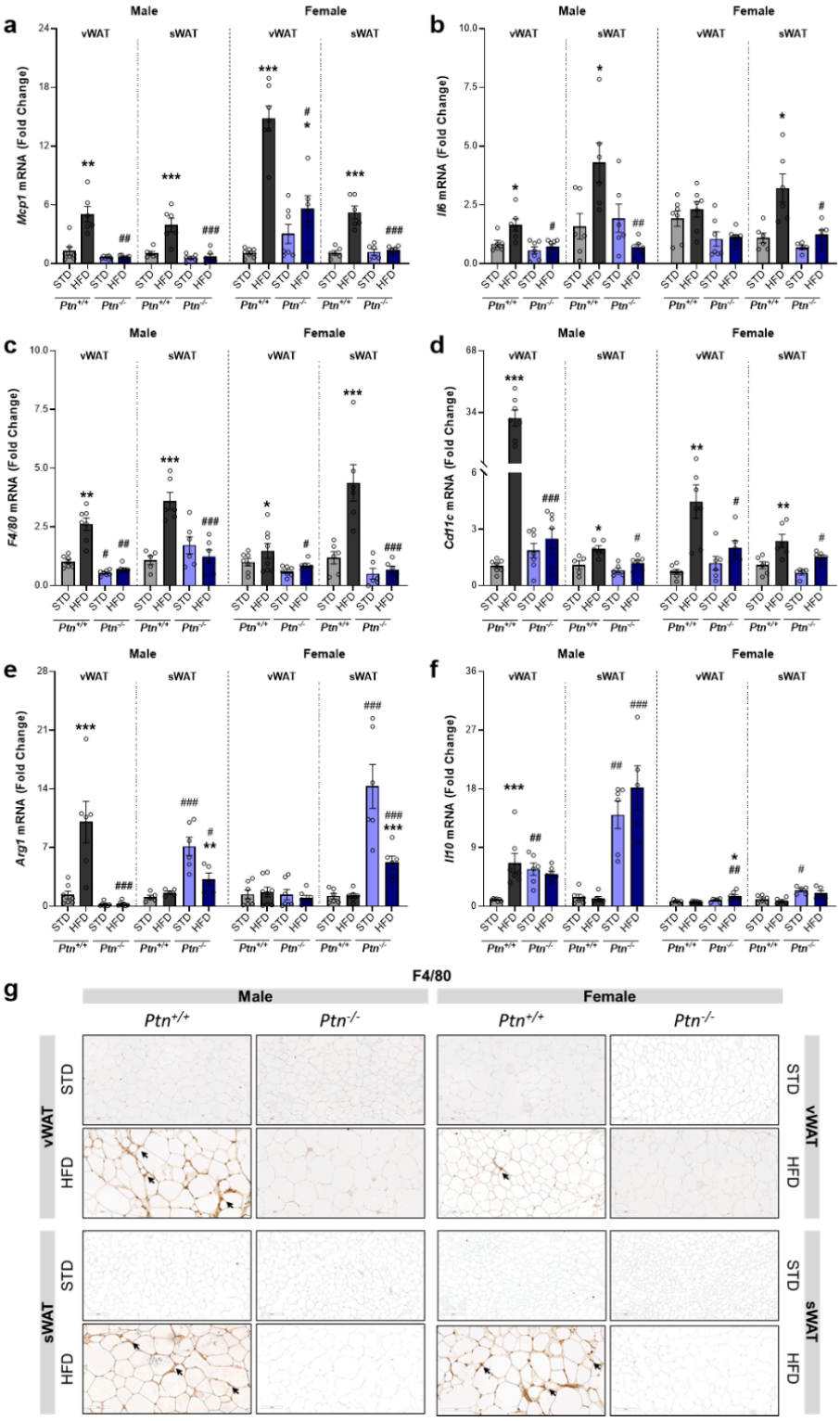


Figure 4

***Ptn* deletion is associated with a differential inflammatory state in visceral and subcutaneous white adipose tissue**. qPCR analyses of (**a**) *F4/80*, (**b**) *Cd11c*, (**c**) *Mcp1*, (**d**) *Il6*, (**e**) *Arg1*, (**f**) *Il10* mRNA, in

visceral (vWAT) and subcutaneous (sWAT) white adipose tissue of male and female *Ptn*$^{+/+}$ (grey bars) and *Ptn*$^{-/-}$ (blue bars) mice (n = 7 mice per group); and (**g**) representative immunohistochemical staining of F4/80 in 3µm-sections of vWAT and sWAT (n = 5 mice per group). Data are expressed as the mean ± SEM of mice per group. **p* < 0.05; ***p* < 0.01; *** *p* < 0.001 for differences in the effect of HFD feeding within *Ptn*$^{+/+}$ or *Ptn*$^{-/-}$ mice. $^{\#}p < 0.05$; $^{\#\#}p < 0.01$; $^{\#\#\#}p < 0.001$ for differences between *Ptn*$^{+/+}$ and *Ptn*$^{-/-}$ genotypes.

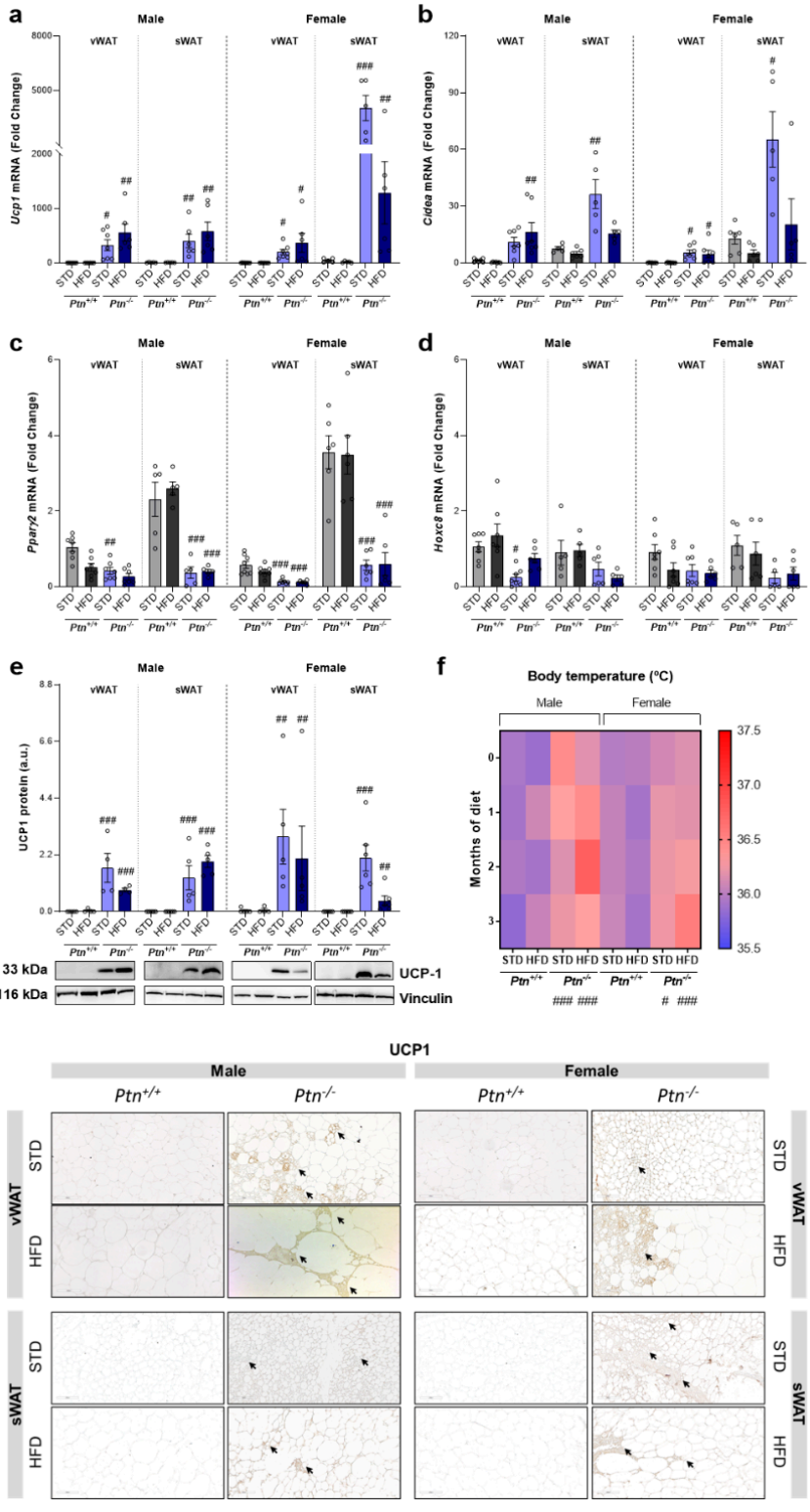
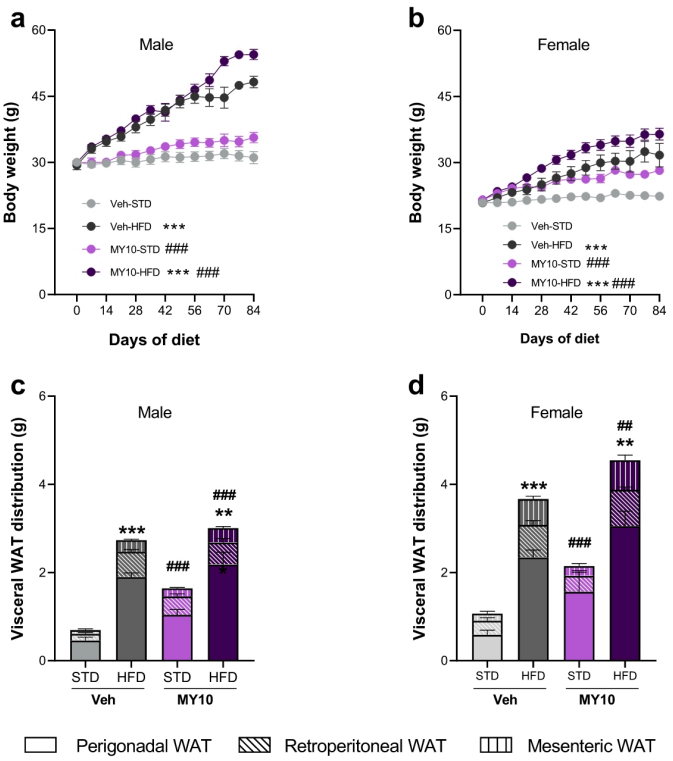


Figure 5

***Ptn* deletion promotes browning of visceral and subcutaneous white adipose tissue.** qPCR analysis of (**a**) *Ucp1*, (**b**) *Cidea*, (**c**) *Pparg2* and (**d**) *Hoxc8* mRNA. (**e**) Western blot analysis of UCP1 protein (normalised to vinculin) in visceral and in subcutaneous adipose tissue of male and female $Ptn^{+/+}$ (grey bars) and $Ptn^{-/-}$ (blue bars) mice. (**f**) Heatmap of body surface temperature (average value of each group at the different months with the diet) (n = 7 mice per group). (**g**) Representative immunohistochemical staining of UCP1 in white adipose tissue (3 μm sections; n = 5 mice per group). Data are presented as mean ± SEM.*$p < 0.05$; **$p < 0.01$; ***$p < 0.001$ for differences due to HFD feeding within each genotype ($Ptn^{+/+}$ or $Ptn^{-/-}$). $^{\#}p < 0.05$; $^{\#\#}p < 0.01$; $^{\#\#\#}p < 0.001$ for differences between genotypes ($Ptn^{+/+}$ vs $Ptn^{-/-}$).



g

Experimental group	Sex	Body weight gain		Food intake	
		Mean	SEM	Mean	SEM
Veh-STD	Male	1,34	0,69	3,33	0,50
Veh-HFD	Male	17,14	2,31	2,67	0,28
MY10-STD	Male	4,88	2,31	3,56	0,31
MY10-HFD	Male	24,22	2,04	2,90	0,22
Veh-STD	Female	1,49	0,73	2,81	0,23
Veh-HFD	Female	13,40	1,75	2,36	0,34
MY10-STD	Female	5,83	1,79	3,13	0,52
MY10-HFD	Female	12,42	5,81	2,67	0,19

Figure 6

Effects of MY10 treatment and HFD feeding on body and white adipose tissue weight. Male and female *Ptn*$^{+/+}$ mice fed with a standard (STD, light symbols) or a high-fat diet (HFD, dark symbols) were treated every other day with vehicle (grey symbols) or MY10 (purple symbols) for three months. Body weight in (**a**) male and (**b**) female mice; distribution of visceral white adipose tissue in (**c**) male and (**d**) female mice; subcutaneous white adipose tissue in (**e**) male and (**f**) female mice fed with a standard chow diet

(STD) or with a high-fat diet (HFD), (**g**) body weight gain and food intake during the 3-month dietary intervention. Data are mean ± SEM of n = 7 mice per group. *$p < 0.05$; **$p < 0.01$; ***$p < 0.001$ for differences in the effect of HFD feeding. $^{\#}p < 0.05$; $^{\#\#}p < 0.01$; $^{\#\#\#}p < 0.001$ for differences between treatments.

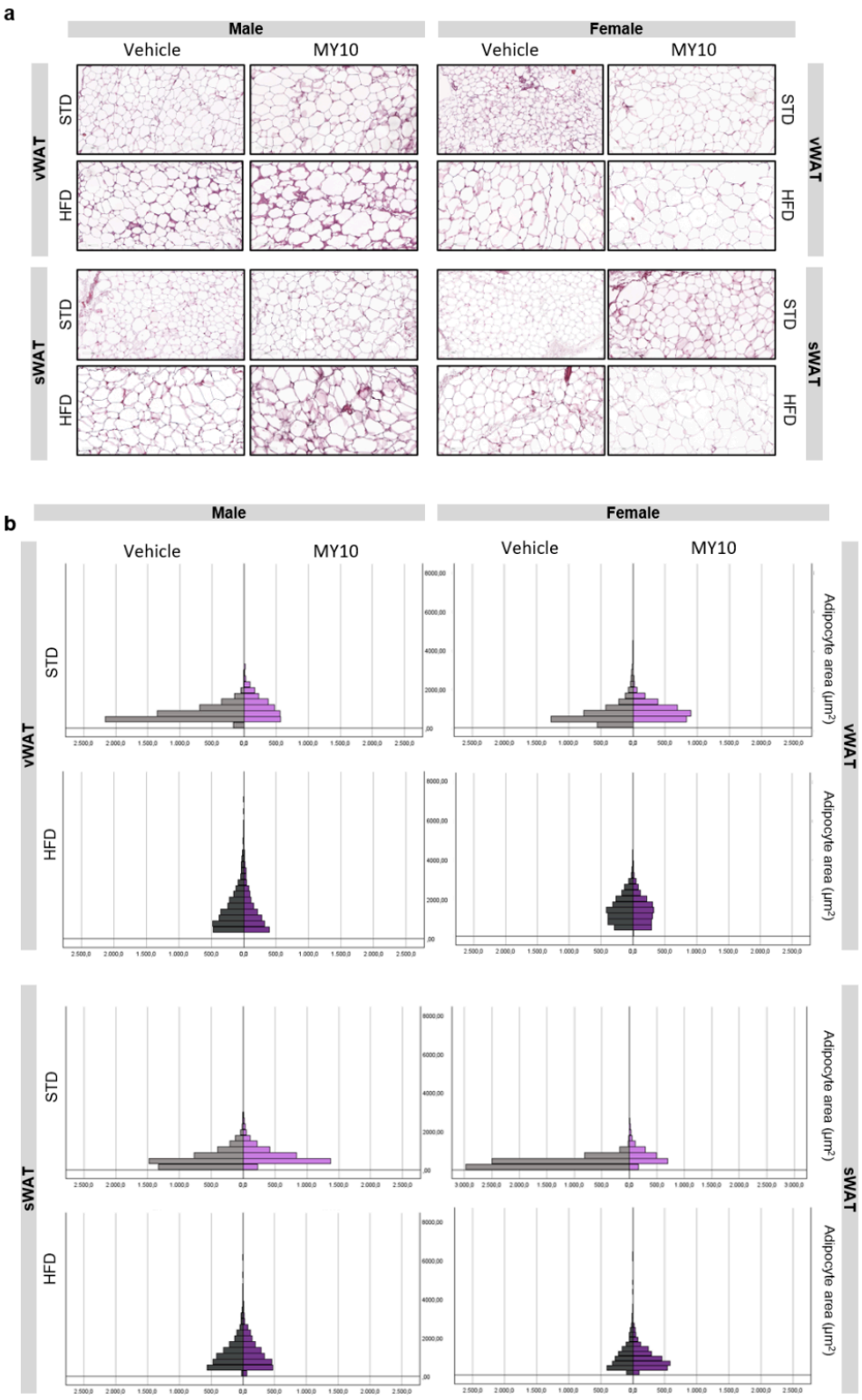


Figure 7

Effects of MY10 treatment and HFD feeding on adipocyte morphology in white adipose tissue. (**a**) Representative sections of visceral perigonadal and subcutaneous adipose tissue stained with haematoxylin-eosin (10× magnification; scale bar 200 µm). (**b**) Distribution of the number and area (µm^2) of adipocytes of perigonadal and subcutaneous adipose tissue of male and female vehicle-treated (grey) and MY10-treated (purple) mice fed a STD or HFD for three months. Data are mean ± SEM of n = 5 mice per group.

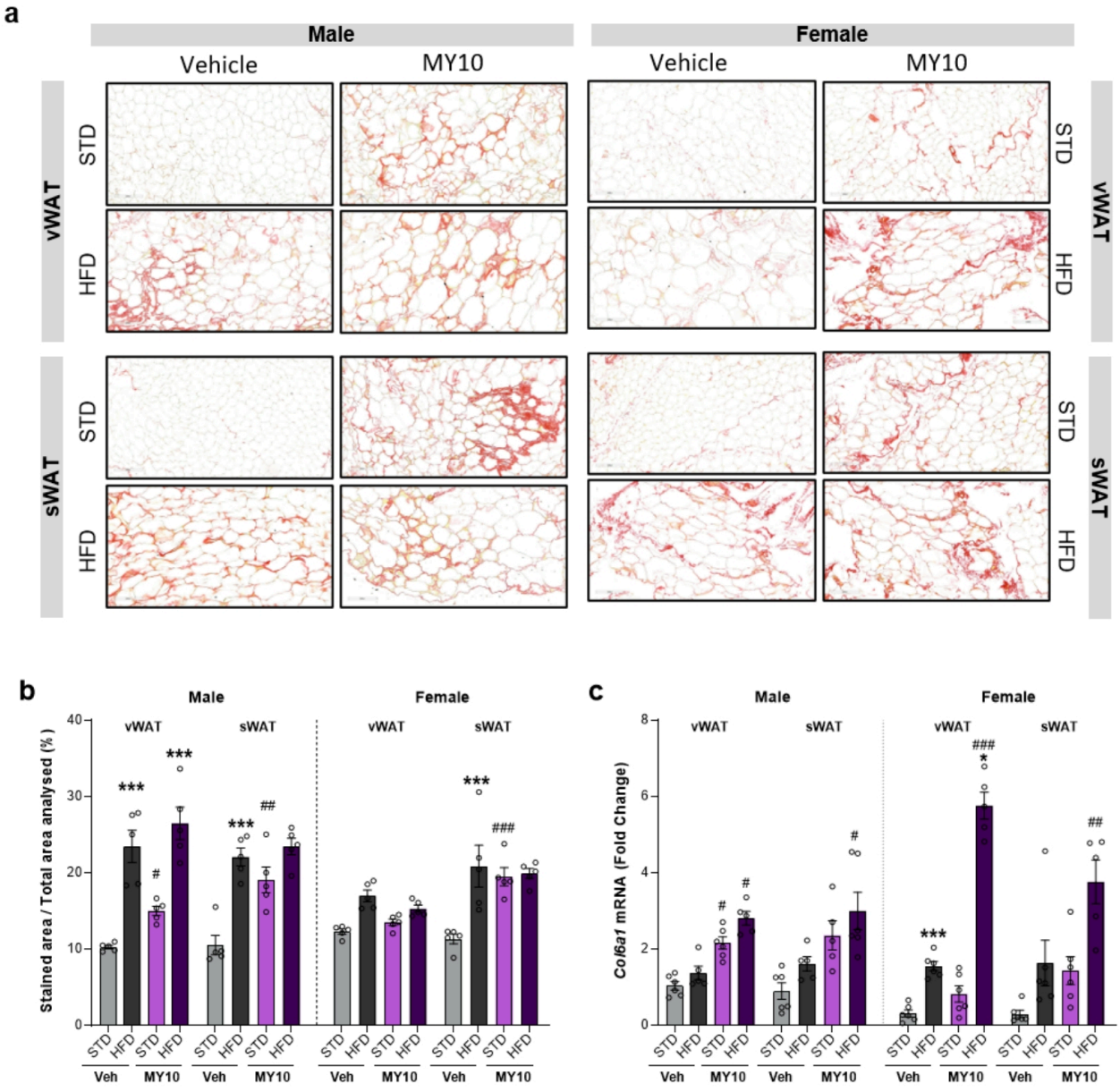


Figure 8

Effects of MY10 treatment and HFD feeding on fibrosis and extracellular matrix remodelling in white adipose tissue. (**a**) Representative sections stained with picrosirius red (10× magnification). (**b**) Quantification of picrosirius red-stained area relative to total tissue area (n= 5 mice per group). (**c**) *Col6a1* mRNA measured by qPCR. Data are mean ± SEM of n = 6 mice per group. * $p < 0.05$; ** $p < 0.01$; *** $p < 0.001$ for the effect of HFD feeding. $^{\#}p < 0.05$; $^{\#\#}p < 0.01$; $^{\#\#\#}p < 0.001$ for differences between treatments.

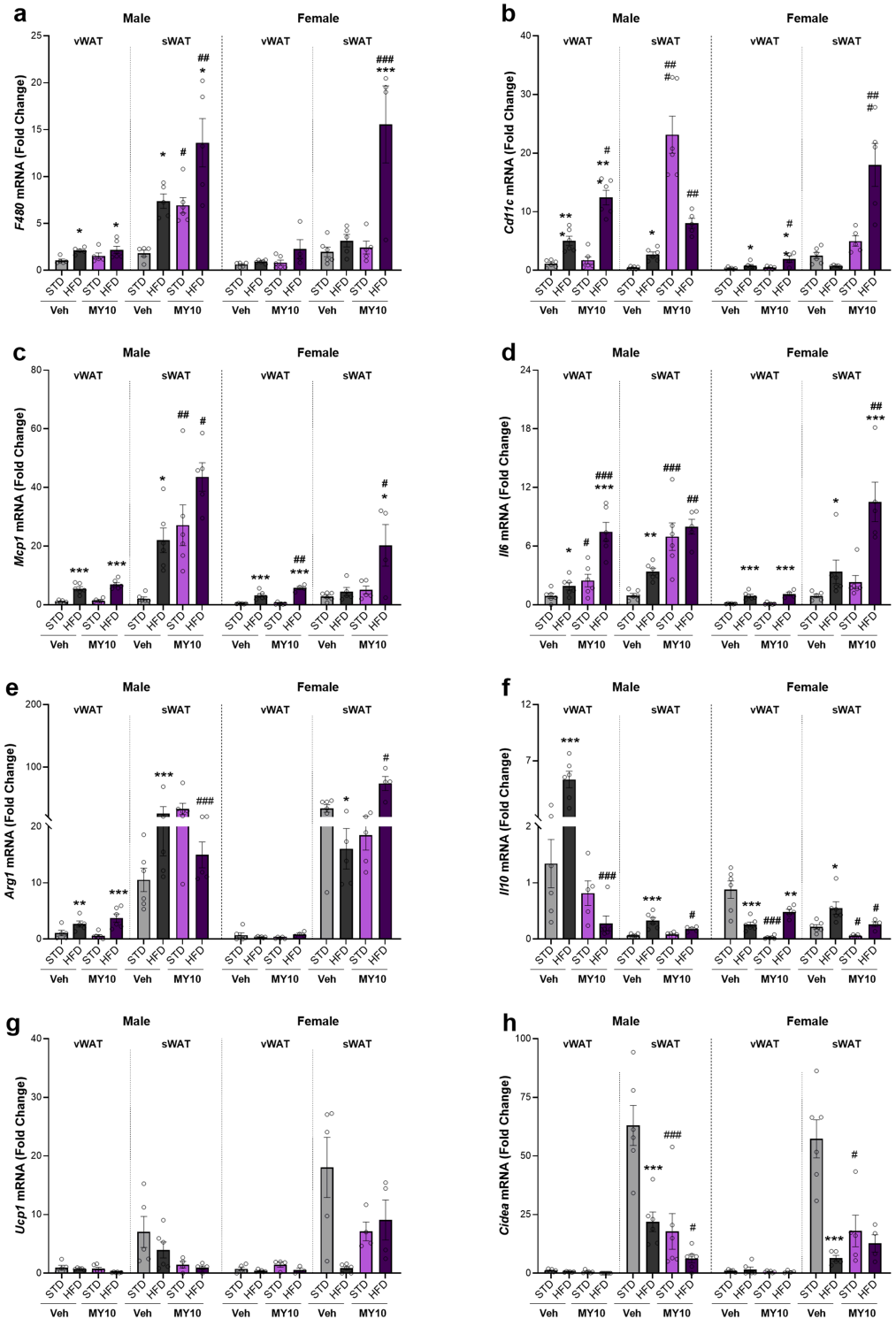


Figure 9

MY10 treatment differentially modulates the expression of genes involved in inflammation and thermogenesis in white adipose tissue. qPCR analysis of (**a**) *F4/80*, (**b**) *Cd11c*, (**c**) *Mcp1,* (**d**) *Il6*, (**e**) *Arg1*, (**f**) *Il10*, (**g**) *Ucp1*, and (**h**) *Cidea* mRNA in visceral and subcutaneous white adipose tissue of male and female $Ptn^{+/+}$ mice treated with vehicle (grey bars) or MY10 (60 mg/kg; purple bars) every other day for three months under a standard diet (STD) or a 60% high-fat diet (HFD). Data are mean ± SEM (n = 7 mice per group). $^{*}p < 0.05$, $^{**}p < 0.01$, $^{***}p < 0.001$ for effects of HFD feeding. $^{\#}p < 0.05$, $^{\#\#}p < 0.01$, $^{\#\#\#}p < 0.001$ for differences between vehicle- and MY10-treated groups.

Supplementary Files

This is a list of supplementary files associated with this preprint. Click to download.

- FulluncroppedblotsSanzCuadradoetal.JPB2026.pdf
- Supplementaryfiguresandtables.docx